ELSEVIER

Journal of Power Sources 81–82 (1999) 709–714

JOURNAL OF POWER SOURCES

www.elsevier.com/locate/jpowsour

X-ray absorption fine structure studies of FeS_2 cathodes in lithium polymer electrolyte batteries

S. Kostov [a,*], M. denBoer [a], E. Strauss [b], D. Golodnitsky [b], S.G. Greenbaum [a], E. Peled [b]

[a] *Physics Department, Hunter College of CUNY, New York, NY 10021, USA*
[b] *School of Chemistry, Tel Aviv University, Tel Aviv, 69978, Israel*

Abstract

We have performed synchrotron X-ray absorption measurements on a series of sealed Li/composite polymer electrolyte (CPE)/FeS_2 cells charged or discharged to various potentials. The Fe K-edge measurements include both the near edge (NEXAFS) and extended (EXAFS) regions. The former provides information on the effective Fe valence while the latter reveals the coordination geometry. Six cells charged and discharged at different conditions were examined. Group A consists of: fully discharged (d-1.1 V), almost fully discharged (d-1.25 V), and partially charged (c-1.85 V) cathodes and group B includes fully charged (c-2.25), almost fully charged (c-2.05 V), and partially discharged (d-1.65 V) cathodes. There appear to be only two distinct Fe environments, one for group A and a dramatically different one for group B. The two different main absorption edge peak shapes observed in groups A and B also reflect these distinct Fe environments. The extended fine structure for group A samples reveals an ordered environment dominated by metallic Fe while the higher Li content group B cathodes are characterized by disorder with only a single Fe–S interatomic distance. Spectral fitting to the experimental data of the d-1.65 cell (in group B) suggests that the compound Li_2FeS_2 is present, with no evidence of FeS. Original cathode material utilization is estimated to be only around 2/3 of full capacity, based on the amount of residual FeS_2 required for satisfactory spectral fitting. On the other hand, no metallic Fe (within detection limits) remains in the recharged cells.

Keywords: Polymer electrolyte; Charge–discharge; Interatomic distance

1. Introduction

Iron disulfide has gained interest as an electrode material in high-capacity lithium batteries. The Li/FeS_2 cell has a high theoretical energy density (about 1270 W h/kg based on 4e/FeS_2) and FeS_2 is inexpensive and nontoxic. The lithium/composite polymer electrolyte (CPE)/pyrite-based battery has many attractive properties. The projected specific energy for 4.0 mA h/cm^2 cathode is 170 W h/kg [1–3]. This all-solid-state thin-film system offers low-cost fabrication, high power and improved safety, as a result of the use of solvent-free components. Recently, rechargeability of the Li/CPE/FeS_2 battery at moderate temperatures (75° to 130°C) was demonstrated [1–4]. Small 1–10 cm^2 area laboratory cells have been developed and characterized. Batteries with 7 μ-thick cathode have exhibited over five hundred 100% DOD cycles with a capacity fade rate of 0.1% [5]. It is established [6] that complete reduction of pyrite (theoretical four electron discharge) leads to the formation of metallic iron and lithium sulfide, Li_2S. Unlike batteries operated at 450°C, pyrite cannot be recharged completely at ambient and moderate temperatures [6,7].

We assume [1–4] that the cathodic reduction of ferrous disulfide proceeds as a multi-stage process, first to Li_2FeS_2 and finally to metallic iron. The first discharge curve for Li/CPE/FeS_2 cell has two plateaus, one at about 1.8 V and another at 1.6 V. Subsequent discharge curves differ from the initial one, indicating that FeS_2 is not formed on charge (Fig. 1a). In the voltage range from 1.1 to 2.25 V, the overall reaction may be considered to be [1–4]:

$$Fe + Li_2S - 2e \rightarrow FeS + 2Li^+ \quad (1)$$

$$FeS + Li_2S \rightarrow Li_2FeS_2 \text{ (chemical step)} \quad (2)$$

$$Li_2FeS_2 - 0.5Li^+ - 0.5e \rightarrow Li_{1.5}FeS_2 (Fe^{2+}, Fe^{3+}) \quad (3)$$

Alternatively, the formation of Li_2FeS_2 may proceed directly without the presence of FeS according to reaction 4

$$Fe + 2Li_2S - 2e \rightarrow Li_2FeS_2 + 2Li^+ \quad (4)$$

* Corresponding author

0378-7753/99/$ - see front matter
PII: S0378-7753(99)00238-4

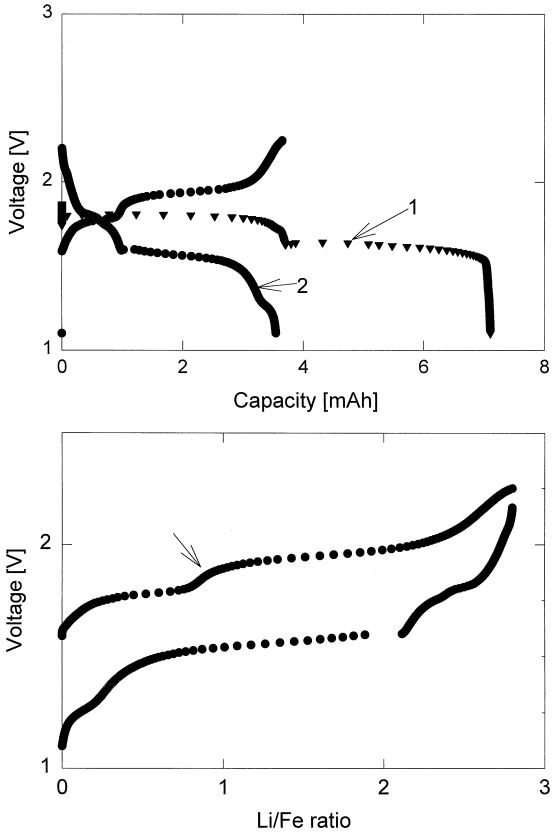

Fig. 1. (a) Typical charge–discharge curves of $Li/CPE/FeS_2$ cell at cycles 1 and 2. (b) Typical charge–discharge of $Li/CPE/FeS_2$ cell at cycle 2. Arrow indicates additional potential step at about 1.85 V.

From the second to fifth discharge, an additional low-voltage plateau, electrochemically atypical for pyrite, has been found at about 1.3 V. Its appearance depends on the operation conditions and it may be associated with the formation of a new phase.

The high-voltage charge region (above 1.95 V) may be attributed to a reversible insertion process (Eq. (3)) and is characterized by a potential dependence on x in Li_xFeS_2. The 1.75-V charge plateau corresponds to three-phase reactions (Eq. (1)), or alternatively Eq. (4). In addition, the charge curves are characterized by an additional potential step at about 1.85 V (Fig. 1b). A sudden voltage jump may be associated either with a slow chemical transition (Eq. (2)) or with the formation of a poorly conducting layer. The generated overpotential may be high enough to enable the initiation of the de-intercalation process (reaction 3), proceeding onto the surface of the cathode active particles. In the inner shell of the lithiated pyrite particles, reactions (1) or (4) are assumed to continue and the three electrochemical processes proceed simultaneously. The proposed intermediate phases formed during the charge–discharge of pyrite in non-aqueous and molten media have been widely studied by electrochemical methods, infrared and Mössbauer spectroscopy, X-ray diffraction, and X-ray absorption fine structure (EXAFS) techniques [4–13]. However, the reaction mechanisms are still not clearly understood, and they may be not directly applicable to our case, as we used a composite polymer electrolyte.

The goal of this work was to identify with the use of synchrotron-based X-ray absorption spectroscopy the different phases formed on charge and discharge of the lithium/composite polymer electrolyte/pyrite battery at 135°C. Six cells charged and discharged at different voltage cutoff were analyzed. The high charge voltage cut-off did not exceed 2.25 V, in order to prevent the formation of polysulfides.

2. Experimental

The electrochemical cells studied comprise a lithium anode, a composite electrolyte consisting of $(LiI)_1P(EO)_{20}$-EC_1 9% v/v Al_2O_3, and a composite FeS_2 cathode which contains about 50% v/v of polymer electrolyte. The electrolytes were prepared from poly(ethylene oxide) (PEO) (Aldrich, average molecular weight 5×10^6), which was vacuum dried at 45° to 50°C for about 24 h. The LiI (Aldrich) was vacuum dried at 200° to 230°C for about 24 h. All subsequent handling of these materials took place under an argon atmosphere in a VAC glove box with water content < 10 ppm. Appropriate quantities of (PEO), LiI, and ethylene carbonate (EC) were dissolved by adding in sequence to analytical reagent grade acetonitrile. The required amount of inorganic filler, such as Al_2O_3 powder (Buehler) with average diameter about 150 Å, was suspended in these solutions. The solutions were stirred for about 24 h before the electrolyte films were cast on a fine polished Teflon support. A high-speed homogenizer was used to ensure the formation of a homogeneous suspension. The solvent was allowed to evaporate slowly and the films were subsequently vacuum dried at 120°C for at least 5 h. The final thickness of the solvent-free films was 100 μm. The cathode foil was prepared by dispersing natural pyrite particles (less than 40 μm size) in a polymer slurry and cast on a Teflon tray. Its theoretical capacity was 10 mA h (based on 11 mg of pyrite in the 0.95 cm^2 45 μm-thick cathode). The theoretical capacity drops to about 7 mA h after the first discharge, corresponding to 2.8 electron reversibility (out of the original four electron reaction).

All investigations were performed in a cell of area 0.95 cm^2 which permitted the sandwiching of a CPE film between the lithium anode and the composite cathode. The cells were held under spring pressure inside a hermetically sealed glass vessel [14]. Before each experiment, cells were equilibrated at 135°C for at least 2 h. Cells were cycled using a Maccor series 2000 battery test system. After charge–discharge the sandwich, containing 10 μm-thick aluminum current collector, pyrite-based composite cathode, polymer electrolyte, lithium anode, and 15 μm

copper current collector was removed from the glass vessel in a glove box and hermetically sealed with 30 μm Kapton film. The total thickness of the sealed cell did not exceed 200 μm.

X-ray absorption measurements of the iron K edge were made at room temperature at beam line X23A2 of the National Synchrotron Light Source at Brookhaven National Laboratory using a double Si(311) monochromator. Both the near-edge X-ray absorption fine structure (NEXAFS) and the extended X-ray absorption fine structure (EXAFS) were measured. The composition and thickness of the cell cathodes allowed the measurements to be performed in transmission mode. All spectra were normalized to the main edge jump. The energy resolution was typically ~0.5 eV, but somewhat smaller shifts were detectable using a reference standard. Fig. 1 illustrates a typical spectrum including both the NEXAFS and EXAFS regions.

3. Results and discussion

Fig. 2 shows the voltage profile of the Li/CPE/FeS_2 cells at first discharge. Two clear plateaus at 1.8 and 1.6 V are apparent. An initial discharge capacity of 7.2 mA h (corresponding to four electrons per mole FeS_2) was obtained, consistent with the conversion of pyrite to Fe and Li_2S. However, the cathode active material utilization was estimated to be only about 70%, probably due to poor interparticle contact. Subsequent cycling of the cells (after the first discharge) was stopped at different stages of charge–discharge as shown in Fig. 3a and b. Six cells were examined by EXAFS: charged to 1.85 V (referred to hereafter as c-1.85); charged to 2.05 V (c-2.05); completely charged to 2.25 V (c-2.25); discharged to 1.65 V (d-1.65); discharged to 1.25 V (d-1.25); and completely discharged to 1.10 V (d-1.10).

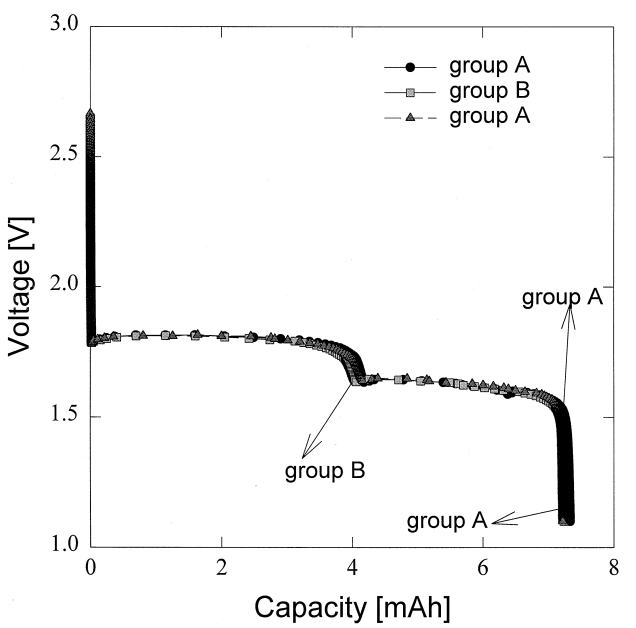

Fig. 2. First discharge of the three experimental Li/CPE/FeS_2 cell; cathode composition: 50% (v/v) FeS_2, 50% (v/v) CPE, cathode thickness 45 μm, CPE composition: LiI $P(EO)_{20}EC_1$ 9% Al_2O_3. Operating conditions: $T = 135$°C, discharge current density = 0.05 mA/cm^2.

Fig. 4 shows the near-edge X-ray absorption region for the cathode series. The six spectra fall into two distinct groups of three cells each, depending on the charge–discharge voltage cutoff. Group A consists of fully discharged (d-1.1 V), almost fully discharged (d-1.25 V), and partially charged (c-1.85 V) cathodes. This group exhibits a somewhat steeper edge jump than group B: fully charged (c-2.25), almost fully charged (c-2.05 V), and partially discharged (d-1.65 V) cathodes. The charge–discharge curves imply group B cathodes must have a Li/Fe ratio of at least 2. Group B exhibits considerably less structure in the near edge region, and are characterized by a distinct loss of long-range order, as indicated by the EXAFS results discussed below. The overall edge position is also shifted to lower energies with increasing lithium content. This well-known effect is due to the decrease in binding energy of the Fe $1s^2$ electrons as the average oxidation is lowered. The derivative plot of the totally discharged cathode (not shown) has two distinct peaks. One is sharp and corresponds in shape and position to metallic iron at ~7111 eV; the other is relatively broad and corresponds to a peak at ~7120 eV in the FeS_2 polycrystalline standard. This evidence of the coexistence of metallic iron and pyrite phases is confirmed by the EXAFS analysis below. The small pre-edge feature near 7112 eV is sharper in the low lithium Group B spectra. This pre-edge feature corresponds to $1s \rightarrow 3d$ transitions which are dipole-forbidden in octahedral symmetry and its strength therefore indicates that the symmetry decreases as Li is removed from the cathode.

The k^3 weighted spectra for the cathode series and the corresponding magnitude of the Fourier transforms are shown in Fig. 5a and b. There are evidently two entirely different structural environments around the absorbing Fe ion. Group B demonstrates very little structure beyond the first peak around 2 Å. Group A, on the other hand, clearly shows long range structure up to more than 5 Å. The spectra within each group of cathodes display the same features, implying a nearly identical Fe environment. To identify which compounds were present in the cathodes, spectra for several possible Fe compounds, including metallic iron, FeS, FeS_2, and Li_xFeS_2, were calculated using the program FEFF 6.01 [15,16] and fitted in r-space to the measured data. A combination of scattering paths corresponding to several coordination shells was required. In the fit, the scattering distances and coordination numbers for all paths were kept fixed at known crystallographic values, while Debye–Waller factors, inner potential E_0, and overall scale factors were allowed to vary. Differences in overall scale factors were attributed to

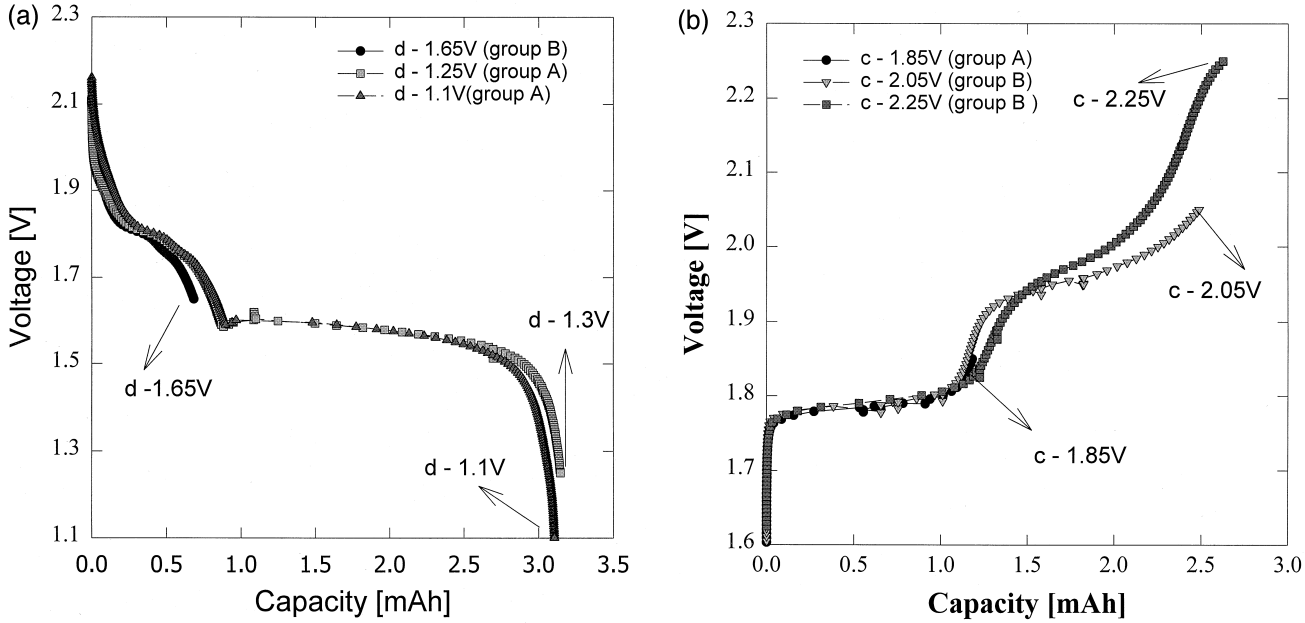

Fig. 3. (a) Second discharge of Li/CPE/FeS_2 cells; cathode composition: 50% (v/v) FeS_2, 50% (v/v) CPE, cathode thickness 45 μm, CPE composition: LiI $P(EO)_{20}EC_1$ 9% Al_2O_3. Operating conditions: $T = 135$°C, discharge current density = 0.300 mA/cm^2. (b) First charge of Li/CPE/FeS_2 cells; cathode composition: 50% (v/v) FeS_2, 50% (v/v) CPE, cathode thickness 45 μm, CPE composition: LiI $P(EO)_{20}EC_1$ 9% Al_2O_3. Operating conditions: $T = 135$°C, charge current density = 0.05 mA/cm^2.

varying proportions of the corresponding compounds and not to changes in coordination. This attribution was possible because we obtained overall scale factors by fitting to experimentally measured spectra of the pure compounds.

Fitting each spectrum in group A gave results which are identical within experimental uncertainty. As shown in Fig. 6 for the d-1.25 (discharged to 1.25 V) cathode, best fit values were obtained from a combination of FeS_2 and metallic iron. The values for the Debye–Waller factors, which measure random disorder about the ideal atomic positions, were somewhat greater for the cathode fit at higher order FeS_2 shells compared to the fit to the experimental standard. This indicates an increase in static disorder with increasing distance within the coexisting pyrite phase. The metallic iron contributions are consistent with those calculated for the foil standard. The overall scale factors corresponding to the two structures, which are free parameters in the fit, are corrected for by the corresponding ones from the fit to the experimental standards, Fe foil and FeS_2 powder. The values thus obtained imply a $35 \pm 5\%$ abundance of FeS_2 and $65 \pm 5\%$ abundance of metallic Fe, in good agreement with estimated cathode utilization on first discharge.

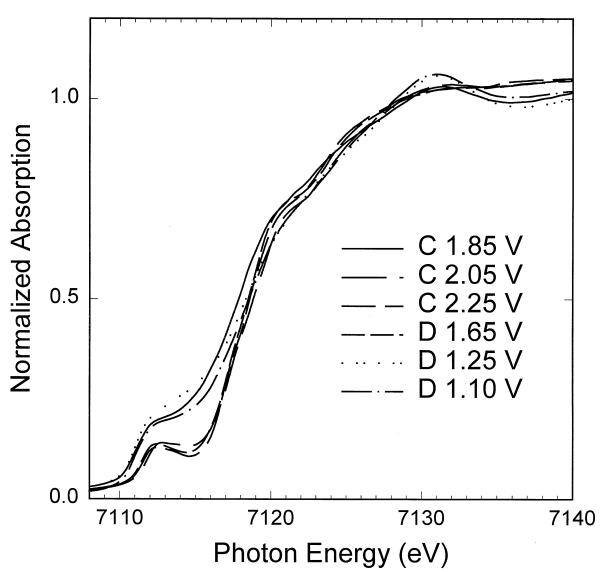

Fig. 4. Near edge (Fe K-edge) X-ray absorption of the Li/CPE/FeS_2 cells.

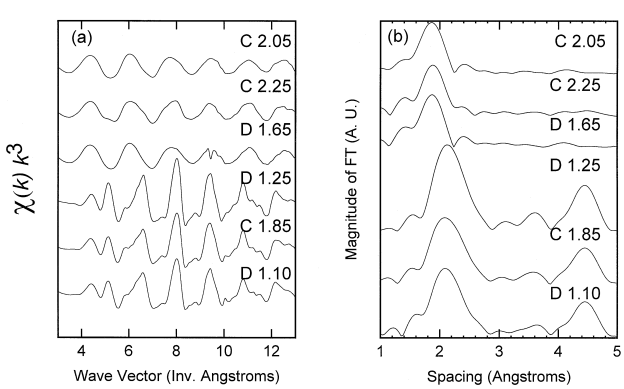

Fig. 5. (a) EXAFS oscillations (k^3-weighted) of Li/CPE/FeS_2 cells. (b) Fourier transform amplitudes (FTA) derived from (a).

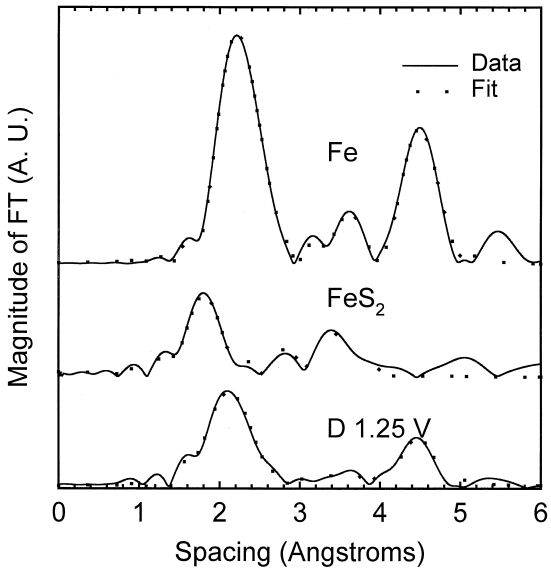

Fig. 6. EXAFS FTA of cell d-1.25 (group A), with Fe and FeS_2 data shown for comparison.

While the FTA of the EXAFS function closely resembles the radial distribution function (RDF) about the absorbing ion, these are not identical. Differences occur for two reasons. First, the peak positions in the FTA are shifted from the 'true' positions of the neighbouring shells due to phase shifts in the scattering. This can in principle be corrected for, using the *k* dependence of the phase shift due to each scatter, which may be obtained from experimental standards or theoretical calculations. Differences are also caused by the fact that the EXAFS signal is averaged over the immediate neighbourhood of the absorbing ion, which may include shells from different compounds or closely spaced shells in the same structure, for example, a distorted octahedral arrangement with long and short bonds. If these distances are too closely spaced and cannot be resolved due to the limited bandwidth of the data, they will appear as a single distorted Gaussian peak. Interatomic spacings calculated from best fits to the data, along with the Debye–Waller factors (σ), are listed in Table 1.

It proved impossible to fit the group B cathodes using coordination numbers and atomic distances obtained from published crystallographic data. As an example we discuss cathode d-1.65, although values obtained for all three spectra were similar. Due to the high correlation of the fit parameters and the *k* range constraint on the number of independent points in the spectra, successive refinements were made keeping some parameters constant and varying others. As shown in Fig. 7, the best fit was obtained by a combination of FeS_2 ($30 \pm 5\%$) and Li_2FeS_2 ($70 \pm 5\%$), in which the Li_2FeS_2 distances were allowed to vary, yielding a nearest-neighbour Fe–S distance of $2.31 \pm .01$ Å, significantly different from the value of 2.37 Å reported for crystalline Li_2FeS_2 [17]. A proper fit to the first Fe–S shells cannot be obtained without the FeS_2 contribution.

Table 1
Interatomic distances and Debye–Waller factors of the Li/CPE/FeS_2 cells and standard compounds

Sample	Shell	r (Å)	σ^2 (Å^2)
FeS_2 electrodes			
1. d-1.25 V (group A)	Fe–S	2.26 ± 0.02	0.004
	Fe–Fe	2.48 ± 0.02	0.004
2. d-1.65 V (group B)	Fe–S[a]	2.26 ± 0.03	0.003
	Fe–S[b]	2.31 ± 0.03	0.004
Fe standards			
1. FeS_2	Fe–S	2.26 ± 0.02	0.004
2. Fe metal	Fe–Fe	2.48 ± 0.02	0.004
Crystallographic data[c]			
1. FeS_2	Fe–S	2.259 ± 0.005	
2. Fe metal	Fe–Fe	2.48	
3. Li_2FeS_2	Fe–S	2.3737 ± 0.004	

[a] From FeS_2 component.
[b] From Li_2FeS_2 component.
[c] From Ref. [17].

The second peak is fit to a Fe–Fe interaction at 2.73 Å. Thus, the main scattering contribution in this group of spectra is due to an Fe environment similar to that of Li_2FeS_2, but with shorter atomic distances. The disagreement between EXAFS measurements on pyrite cathodes believed to contain Li_2FeS_2 and crystallographic Li_2FeS_2 has been noted previously [13]. The absence of longer range peaks due to the pyrite may be due to modest disorder of the FeS_2 structure in the lithiated composite cathode, which would broaden the Fe–Fe peaks above 3 Å.

Because FeS is a possible intermediate compound in the c-2.05 and d-1.65 cathodes (Eq. (1)), Fig. 7 shows the effect on the fit of including 10% and 20% FeS (substituted for the Li_2FeS_2). It is clear that including FeS

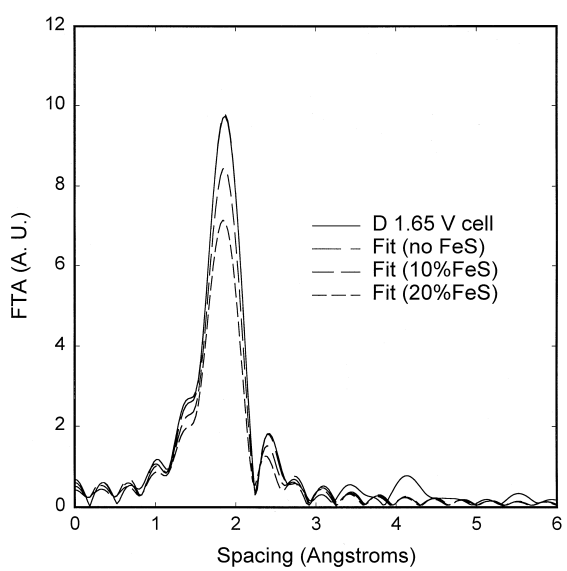

Fig. 7. EXAFS FTA of cell d-1.65 (group B), including fits to Li_2FeS_2 + FeS_2, with amounts as indicated of FeS included in the fit.

only worsen the fit (the simulated spectral width and amplitude must both fit the experimental data). Thus, significant amounts of FeS (more than several percent) can be ruled out. It is also important to see if metallic Fe, the dominant feature in the low Li Group A cathodes, is detectable in the higher Li cathodes. For the d-1.65 and c-2.05 samples, an upper limit of 5% metallic Fe can be set on the basis of. the observed degradation of the fit if more is included.

4. Conclusions

EXAFS and NEXAFS measurements of sealed Li/CPE/pyrite batteries provide evidence that the dominant cathode component of the cells charged up to 1.85 V is Li_2FeS_2, with no evidence of FeS. The cathode discharged to 1.10 V contains a mixture of $65 \pm 5\%$ metallic iron and $35 \pm 5\%$ pyrite, due to incomplete utilization of active cathode material. Upon recharging, there is no evidence (beyond the detection limit of $\sim 5\%$) of metallic Fe remaining. It would be of interest to extend these studies to cells charged or discharged to Li contents between those of c-1.85 of group A and d-1.65 of group B, in order to observe more closely the transition between Fe environments characteristic of these groups. It would also be useful to examine cells that have undergone more extensive cycling.

Acknowledgements

This research was supported by the U.S. Department of Energy and the Israeli Ministry of Energy.

References

[1] E. Peled, D. Golodnitsky, G. Ardel, J. Lang, Y. Lavi, in: S.P. Wolsky, N. Marincic (Eds.), Proceedings of the 11th International Seminar on Primary and Secondary Battery Technology and Applications, Florida, Educational Seminar, March 1994.
[2] E. Peled, D. Golodnitsky, G. Ardel, J. Lang, Y. Lavi, J. Power Sources 54 (1995) 496–500.
[3] E. Peled, D. Golodnitsky, E. Strauss, J. Lang, Y. Lavi, Electrochimica Acta, 1997, in press.
[4] E. Strauss, D. Golodnitsky, Y. Lavi, E. Peled, L. Burstein, Y. Lareah, The Joint Meeting of the Electrochemical Society, Proceedings. Paris, France, 1997.
[5] E. Strauss, A. Blum, G. Ardel, Y. Lavi, D. Golodnitsky, E. Peled, 9th International Meeting on Lithium Batteries, Abstracts, Edinburgh, Scotland, 1998.
[6] M.B. Clark, Lithium–iron disulfide cells, in: J.P. Gabano (Ed.), Lithium Batteries, Academic Press, New York, 115, 1983.
[7] R. Fong, J.R. Dahn, C.H.W. Jones, J. Electrochem. Soc. 136 (1989) 11.
[8] R. Fong, C.H.W. Jones, J.R. Dahn, J. Power Sources 26 (1989) 333.
[9] C.H.W. Jones, P.E. Kovacs, R.D. Sharma, R.S. McMillan, J. Phys. Chem. 94 (1990) 832.
[10] R. Brec, E. Prouzet, G. Ouvrard, J. Power Sources 26 (1989) 325.
[11] P. Gard, C. Sourisseau, G. Ouvrard, R. Brec, Solid State Ionics 20 (1986) 231.
[12] K. Hansen, K. West, The Joint Meeting of the Electrochemical Society, Proceedings, Paris, France, 125 (1997).
[13] D.A. Totir, I.T. Bae, Y. Hu, M.R. Antonio, M.A. Stan, D.A. Scherson, J. Phys. Chem. B 101 (1997) 9751.
[14] D. Golodnitsky, G. Ardel, E. Strauss, E. Peled, Y. Lareah, Yu. Rosenberg, J. Electrochem. Soc. 144 (1997) 3484.
[15] J.J. Rehr, R.C. Albers, S.I. Zabinsky, Phys. Rev. Lett. 69 (1992) 3397.
[16] Ab initio Multiple-Scattering X-ray Absorption Fine Structure and X-ray Absorption Near Edge Structure Code, Copyright 1992, 1993, FEFF Project, Department of Physics, FM-15 University of Washington, Seattle, WA 98195.
[17] R.J. Batchelor, F.W.B. Einstein, C.H.W. Jones, R. Fong, J.R. Dahn, Phys. Rev. B 37 (1988) 3699.